

Topological phase diagrams of exactly solvable non-Hermitian interacting Kitaev chains

Sharareh Sayyad^{1,*} and Jose L. Lado²

¹Max Planck Institute for the Science of Light, Staudtstraße 2, 91058 Erlangen, Germany

²Department of Applied Physics, Aalto University, FI-00076 Aalto, Espoo, Finland

(Dated: February 28, 2023)

Many-body interactions give rise to the appearance of exotic phases in Hermitian physics. Despite their importance, many-body effects remain an open problem in non-Hermitian physics due to the complexity of treating many-body interactions. Here, we present a family of exact and numerical phase diagrams for non-Hermitian interacting Kitaev chains. In particular, we establish the exact phase boundaries for the dimerized Kitaev-Hubbard chain with complex-valued Hubbard interactions. Our results reveal that some of the Hermitian phases disappear as non-Hermiticity is enhanced. Based on our analytical findings, we explore the regime of the model that goes beyond the solvable regime, revealing regimes where non-Hermitian topological degeneracy remains. The combination of our exact and numerical phase diagrams provides an extensive description of a family of non-Hermitian interacting models. Our results provide a stepping stone toward characterizing non-Hermitian topology in realistic interacting quantum many-body systems.

Introduction. Many-body interactions play a crucial role in Hermitian quantum systems. The emergent correlation effects in these systems give rise to a variety of collective phenomena, such as spontaneous symmetry breaking [1–4], phase transitions [5–8], and the emergence of fractionalized quasiparticles [9–12]. Understanding these rich phenomena often requires the combination of analytical and numerical techniques due to the scarcity of exact solutions for many-body models. Nonetheless, especially in one-dimensional systems, analytical solutions in specific regimes are attainable [13–18]. Away from these parameter regimes, employing various numerical methods [13, 19–25] allows unveiling the underlying physics of many-body systems in generic scenarios.

The presence of losses and dissipation in real systems provide natural platforms realizing non-Hermitian models [26–35]. Non-Hermitian quantum models have risen as a new paradigm to manipulate and interpret various emergent phenomena [36, 37]. Here, Non-Hermiticity emerges as the effective description [38–45] of out-of-equilibrium and open quantum systems, e.g., in superconducting qubits [46–48], giving rise to various phenomena absent in the Hermitian counterpart. Paradigmatic examples are occurrence of various non-Hermitian degeneracies [49–53] and non-Hermitian (bulk) skin states [54, 55]. Both of these phenomenologies are mainly explored in effectively single-particle non-Hermitian Hamiltonians while non-Hermitian many-body effects have remained relatively unexplored, partly due to limitations of numerical methods [56–61]. In particular, recent efforts have addressed one-dimensional non-Hermitian fermionic [62–67] and bosonic [68, 69] Hubbard models. Here, the non-Hermiticity is incorporated by having nonreciprocal hopping [62], complex Hopping [64], or complex Hubbard in-

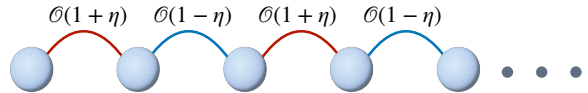


Figure 1. Schematic illustration of a 1D dimerized Kitaev-Hubbard chain with dimerized hopping t , pairing Δ , and complex-valued Hubbard interaction $U - i\delta$. Here, η denotes the dimerization parameter and $\mathcal{O} \in \{t, \Delta, U, \delta\}$.

teraction [63, 65, 66]. The latter form of non-Hermiticity provides effective descriptions for experiments on open quantum systems with two-body loss [70–73].

In this Letter, combining exact analytical results and numerical calculations, we establish the phase diagram of a family of non-Hermitian Kitaev chains [40, 74–76]. Our interacting model consists of a complex-valued many-body interaction that may host Majorana modes, in particular, realizable in an array of Josephson junctions [77]. Our results reveal that, depending on the relative couplings, non-Hermitian interacting phases with topological degeneracies emerge in the system. We show how increasing the non-Hermiticity parameters affect some of the many-body topological phases. We furthermore present that the topological degeneracies of the model remain in the non-analytically solvable regime by numerically solving the interacting problem.

Model. The Hamiltonian for the non-Hermitian dimerized Kitaev-Hubbard chain, schematically shown in Fig. 1, reads

$$\begin{aligned} \mathcal{H} = & - \sum_{j=1}^{L-1} \left[t_j (c_j^\dagger c_{j+1} + c_{j+1}^\dagger c_j) + \Delta_j (c_j^\dagger c_{j+1}^\dagger + c_{j+1} c_j) \right] \\ & + \sum_{j=1}^{L-1} (U_j - i\delta_j) (2n_j - 1) (2n_{j+1} - 1) - \mu \sum_{j=1}^L (n_j - \frac{1}{2}), \end{aligned} \quad (1)$$

* sharareh.sayyad@mpl.mpg.de

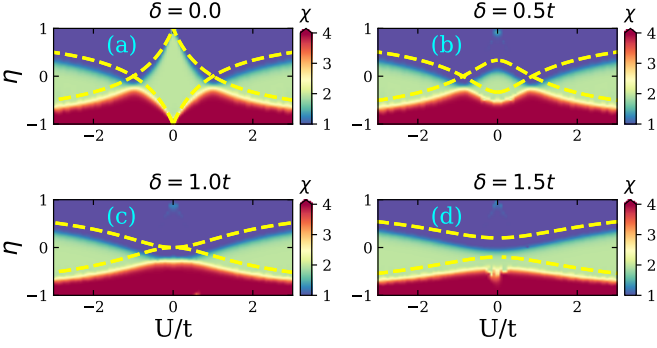


Figure 2. Phase diagrams of the non-Hermitian Hamiltonian and associated orders of degeneracies on the $(U/t - \eta)$ plane at $\mu = 0$ and $\Delta = t$. Non-Hermiticity parameter is set to $\delta/t = 0$ (a), 0.5 (b), 1.0 (c), 1.5 (d). The yellow dashed lines display the exact phase boundaries given by Eq. (6). The heat map shows the degeneracies obtained numerically for a chain with length $L = 16$, shown in red, green, and blue, respectively, for fourfold, twofold, and no degeneracies.

where L denotes the length of the chain, c_j^\dagger (c_j) creates (annihilates) an spinless fermion at site j associated with the fermion density $n_j = c_j^\dagger c_j$. Here μ adjusts the onsite energy, and t_j , Δ_j and U_j are, respectively, real-valued site-dependent hopping amplitude, superconducting pairing amplitude, and Hubbard interaction. The dimerized parameter $\mathcal{O}_j \in \{t_j, \Delta_j, U_j, \delta_j\}$ for $1 \leq j \leq L$ reads

$$\mathcal{O}_j = \begin{cases} \mathcal{O}(1 - \eta), & j \bmod 2 = 0, \\ \mathcal{O}(1 + \eta), & j \bmod 2 = 1, \end{cases} \quad (2)$$

where η is the real-valued dimerization parameter and $\mathcal{O} \in \{t, \Delta, U, \delta\}$ stands for site-independent parameters; see also Fig. 1.

The Hamiltonian in Eq. (1) at $\mu = 0$ remains invariant under $c_j \rightarrow (-1)^j c_j^\dagger$ which enforces the charge conjugation symmetry. We note that respecting this symmetry ensures that eigenvalues of the Hamiltonian come in complex-conjugate pairs making this model not directly realizable in open quantum systems [39], which can be resolved by a negative imaginary shift of all eigenvalues [78]. Nevertheless, preserving the charge conjugation symmetry in Hermitian models ($\delta = 0$) at the symmetric point $\Delta = t$ allows calculating exact phase diagrams for arbitrary η [13–17]. In the following, we present that there exists an analytical solution for the non-Hermitian model when the charge conjugation symmetry is respected, i.e., at $\mu = 0$ and $\Delta = t$. When $\Delta \neq t$ or $\mu \neq 0$, we compute the topological phase diagram numerically.

Exact solution at $\mu = 0$ and $\Delta = t$. To obtain the exact phase diagram of the model Hamiltonian at $\mu = 0$, we employ two Jordan-Wigner transformations and one spin rotation; see the Supplemental materials (SM) for details [79]. This procedure map our initial non-Hermitian interacting Hamiltonian into a non-

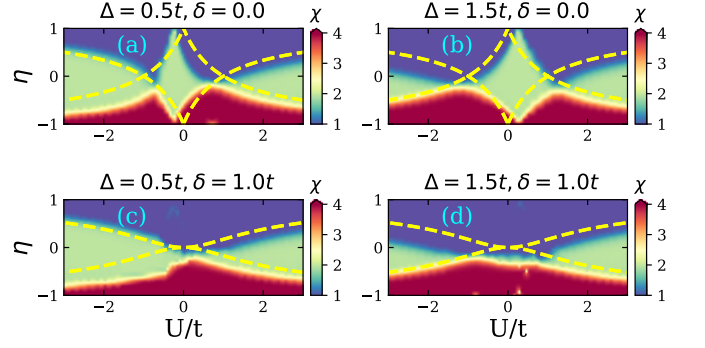


Figure 3. Phase diagrams of the non-Hermitian Hamiltonian and associated orders of degeneracies on the $(U/t - \eta)$ plane at $\mu = 0$ and $\Delta \neq t$. The heat map corresponds to the degeneracies obtained numerically for a system with $L = 16$. The superconducting pairing amplitude and non-Hermiticity are set to $(\Delta/t, \delta) = (0.5, 0.0)$ (a), $(1.5, 0.0)$ (b), $(0.5, 1.0)$ (c), $(1.5, 1.0)$ (d). The yellow dashed lines are phase boundaries at $\Delta = t$ and are shown as a guide for eye.

Hermitian quadratic fermionic model given by

$$\mathcal{H} = \sum_j -t_j \left[f_{j+1}^\dagger f_j + f_j^\dagger f_{j+1} + f_j^\dagger f_{j+1}^\dagger + f_{j+1} f_j \right] + \sum_j \tilde{U}_j \left[f_{j+1}^\dagger f_j + f_j^\dagger f_{j+1} - f_j^\dagger f_{j+1}^\dagger - f_{j+1} f_j \right], \quad (3)$$

which in the momentum-space casts

$$\mathcal{H} = \sum_k (-t + \tilde{U}) \left[z_k f_{kB}^\dagger f_{kA} + z_k^* f_{kA}^\dagger f_{kB} \right] - \sum_k (t + \tilde{U}) \left[w_k f_{-kA}^\dagger f_{kB} + w_k^* f_{kB}^\dagger f_{-kA} \right], \quad (4)$$

where $\tilde{U} = U - i\delta$. Diagonalizing this Hamiltonian, we obtain the energy spectrum of this four-band system given by

$$\frac{\Lambda_k^2}{4} = \begin{cases} \tilde{U}^2(1 + \eta)^2 + t^2(1 - \eta)^2 - 2t\tilde{U}(1 - \eta^2) \cos(k), \\ \tilde{U}^2(1 - \eta)^2 + t^2(1 + \eta)^2 - 2t\tilde{U}(1 - \eta^2) \cos(k), \end{cases} \quad (5)$$

where $\tilde{U}^2 = U^2 - \delta^2 - 2i\delta U$. As eigenvalues of our system appear in complex-conjugate pairs, due to the charge-conjugation, zero modes in Λ_k emerge when $\text{Re}[\Lambda_k] = 0$ at

$$\frac{U}{t} = \sqrt{\frac{\delta^2}{t^2} - \frac{(1 \pm \eta)^2}{(1 \mp \eta)^2}}, \quad (6)$$

which is obtained at $k = \pm\pi/2$. In the Hermitian limit ($\delta = 0$), Eq. (6) reproduces the Hermitian results [13–17]. Eq. (6) shows the boundaries between various phases in our system, presented in yellow dashed lines in Fig. 3. These boundaries delineate phases with four-fold, twofold, and no degeneracies, respectively, shown

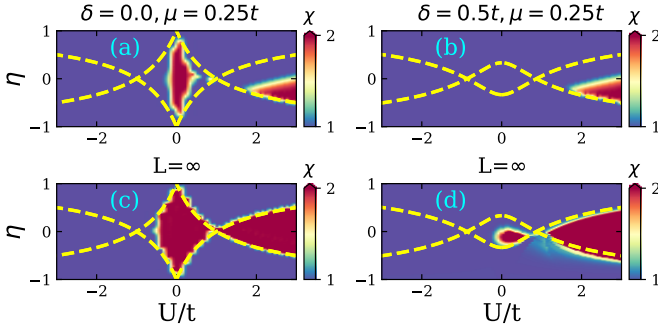


Figure 4. Phase diagrams of the non-Hermitian Hamiltonian and associated orders of degeneracies on the $(U/t - \eta)$ plane with $\mu \neq 0$. The superconducting pairing amplitude is set to $\Delta = t$. The chain size is set to $L = 16$ in (a,b), and extrapolated data in the thermodynamic limit are shown in (c,d). The yellow dashed lines are phase boundaries at $\mu = 0$ and are shown as a guide for the eye. We took $\delta, \mu = 0, 0.25t$ in (a,c) and $\delta, \mu = 0.5, 0.25t$ in (b,d)

in red, green, and blue in Fig. 2. The order of degeneracy is determined by $\chi = \sum_{i=0}^L \exp[-\lambda|\varepsilon_i - \varepsilon_0|]$. This quantity measures the degeneracy between first ε_0 and the i the smallest eigenvalue ε_i within the energy resolution of $1/\lambda (= 0.05)$. Here the eigenvalues are calculated using the numerical exact diagonalization method. The difference between the numerical boundaries and the exact solution should be attributed to the finite size effect. In the thermodynamic limit ($L = \infty$), one can recover the exact phase boundaries; see the SM [79]. The topological superconducting phase residing in the boundaries surrounding $U = 0$ [80] shrinks as non-Hermiticity increases. At the critical value $\delta = t$, this topological phase fades away, resulting in the mixing of other two-fold degenerate phases. It is also worth noting that the exact phase boundaries in Eq. (6) are associated with transitions between non-Hermitian spectra with different types of the gap in the non-Hermitian effective model in Eq. (4); see also the SM [79].

Many-body Majorana edge modes. To identify Majorana modes in our model, in the next step, we rewrite the Hamiltonian in Eq. (3) in terms of Majorana fermions $\Upsilon_j^A = f_j^\dagger + f_j$ and $\Upsilon_j^B = i(f_j^\dagger - f_j)$. The Hamiltonian then reads

$$\mathcal{H} = i \sum_j \left[t_j \Upsilon_j^B \Upsilon_{j+1}^A + \tilde{U}_j \Upsilon_j^A \Upsilon_{j+1}^B \right]. \quad (7)$$

We note that interactions and hopping amplitudes between the same sublattices or within each unit cell vanish. Hence, Eq. (7) can be decoupled into two independent non-interacting Kitaev chains with length $L/2$ such that $\mathcal{H} = \mathcal{H}_I + \mathcal{H}_{II}$ where

$$\mathcal{H}_I = \sum_{j=1}^{L/2} \left[-it_{2j} \Phi_{I,j+1}^A \Phi_{I,j}^B + i\tilde{U}_{2j-1} \Phi_{I,j}^A \Phi_{I,j}^B \right], \quad (8)$$

$$\mathcal{H}_{II} = \sum_{j=1}^{L/2} \left[i\tilde{U}_{2j} \Phi_{II,j+1}^B \Phi_{II,j}^A - it_{2j-1} \Phi_{II,j}^B \Phi_{II,j}^A \right], \quad (9)$$

with $\Phi_{I,j}^A = \Upsilon_{2j-1}^A$, $\Phi_{I,j}^B = \Upsilon_{2j}^B$, $\Phi_{II,j}^B = \Upsilon_{2j-1}^B$, and $\Phi_{II,j}^A = \Upsilon_{2j}^A$. Introducing Majorana particles from the electron operators as $\gamma_j^A = c_j^\dagger + c_j$ and $\gamma_j^B = i(c_j^\dagger - c_j)$, one can show that Υ operators are products of γ operators such that [15, 17, 81–84]

$$\Upsilon_j^A = \begin{cases} \prod_{k=\text{odd}}^{j-1} [i\gamma_k^B \gamma_{k+1}^A] \gamma_j^A, & j = \text{odd}, \\ \prod_{k=\text{odd}}^{j-3} [i\gamma_k^A \gamma_{k+1}^B] (i\gamma_{j-1}^A \gamma_j^A), & j = \text{even}, \end{cases} \quad (10)$$

$$\Upsilon_j^B = \begin{cases} \prod_{k=\text{odd}}^{j-2} [i\gamma_k^A \gamma_{k+1}^B] i\gamma_j^A \gamma_j^B, & j = \text{odd}, \\ \prod_{k=\text{odd}}^{j-1} [i\gamma_k^B \gamma_{k+1}^A] \gamma_j^B, & j = \text{even}. \end{cases} \quad (11)$$

These relations keep the Majorana anti-commutation relations unchanged, i.e., $\{\Upsilon_i^\alpha, \Upsilon_j^\beta\} = \{\gamma_i^\alpha, \gamma_j^\beta\} = 2\delta_{i,j}\delta^{\alpha,\beta}$. We note that Υ operators, which are comprised of odd (even) number of Majorana fermions (γ s), belong to subsystem I (II) described by \mathcal{H}_I (\mathcal{H}_{II}).

The quadratic Hamiltonian in Eq. (7) may host two types of boundary modes (\mathcal{Q}). These boundary modes are constructed from linear combinations of $\Phi_{I/II}^{A/B}$ operators, i.e., $\mathcal{Q}_\beta^\alpha = \sum_{j \geq 0} a_{\beta,j} \Phi_{\beta,j}^\alpha$ with $\alpha = A, B$ and $\beta = I, II$. As \mathcal{Q} consists of higher-order multiple Majorana fermions, it is dubbed "many-body Majorana operator" [84]. In the Hermitian limit, \mathcal{Q} operators are conserved, $[\mathcal{H}, \mathcal{Q}] = 0$, and using the iteration procedure, one can determine the coefficients (a) as [15, 84, 85]

$$a_{I,j} = - \left(\frac{U(1+\eta)}{t(1-\eta)} \right)^{j-1}, \quad a_{II,j} = - \left(\frac{t(1+\eta)}{U(1-\eta)} \right)^{j-1}. \quad (12)$$

In non-Hermitian systems, the operator \mathcal{O} is conserved if it satisfies $[\mathcal{H}_R, \mathcal{O}] = [\mathcal{H}_I, \mathcal{O}] = 0$ where $\mathcal{H} = \mathcal{H}_R + i\mathcal{H}_I$ [53]. We note that based on the structure of $\mathcal{H}_{I/II}$ in Eqs. (8) and (9), $[\mathcal{H}_I, \mathcal{O}] = 0$ is by construction satisfied and fulfilling $[\mathcal{H}_R, \mathcal{O}] = 0$ results in obtaining Eq. (12). Hence, the boundary modes in our non-Hermitian system are continuously ($\delta \rightarrow 0$) connected to the zero-energy boundary modes.

The Majorana boundary mode \mathcal{Q}_I consists of odd numbers of higher-order Majorana operators (γ) is fermionic and satisfies $\{\mathcal{Z}_2, \mathcal{Q}_I\} = 0$, in the infinite chain limit [85]. However, the \mathcal{Q}_{II} mode comprises even numbers of higher-order Majorana operators (γ) is bosonic as $[\mathcal{Z}_2, \mathcal{Q}_{II}] = 0$ [14, 15, 84]. Regions with fourfold degeneracies in Fig. 2 host both ($\mathcal{Q}_I, \mathcal{Q}_{II}$). The topological superconducting phase enclosing $U = 0$ merely hosts \mathcal{Q}_I , in agreement with Hermitian noninteracting intuition [80]. The other two twofold degenerate phases accommodate \mathcal{Q}_{II} .

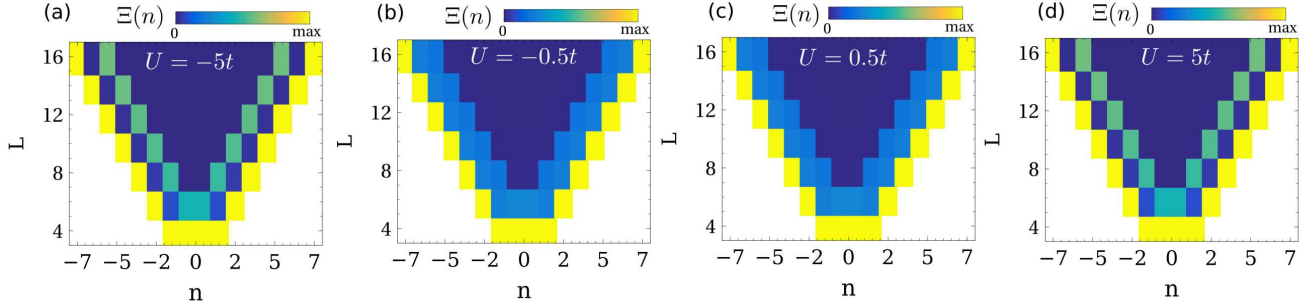


Figure 5. Spatial distribution of the zero modes for different system lengths for the non-Hermitian model computed with the local response function given by Eq. (13). It is observed that both in the presence of repulsive and attractive interactions, an edge response appears, accounting for the topological degeneracy of the model. The edge excitations emerge both in the case of two-fold (a,d) and four-fold (b,c) degeneracy. We took $\mu = 0$, $\Delta = t$, $\eta = -0.6$ and $\delta = 0.5t$.

Beyond exact solutions. Let us now present the phase diagram of our system away from the integrable regime $\Delta = t$ and $\mu = 0$. First, we consider $\Delta/t \in \{0.5, 1.5\}$ and plot the associated phase diagrams with $\delta \in \{0.0, 1.0\}$ in Fig. 3 for a finite size system with $L = 16$. Similar to the phase diagram of the system at $\Delta = t$, we witness phases with fourfold, twofold, and no degeneracies. Comparing the exact phase boundaries at $\Delta = t$, in yellow dashed lines, with boundaries of regions with $2n$ fold degeneracies, in red or green, we identify deformation of the phase boundaries toward $U < 0$ (> 0) for $\Delta < t$ ($> t$).

At finite chemical potential and $\delta = 0$, all fourfold degeneracies are lifted, and merely phases with twofold degeneracies remain in the phase diagram; see Fig. 4. The Hermitian phase boundary $U = -0.5t$ at $\eta = 0$ is consistent with previous calculations on the Kitaev-Hubbard chain [86]; see panels (a) at $L = 16$, (c) in the thermodynamics limit and the SM [79]. Witnessing merely twofold degeneracies in phases with $U > 1$ in the Hermitian limit also persists as non-Hermiticity is increased; see Fig. 4(b) at $L = 16$. While no portion of the topological superconducting phase, region encircling $U = 0$, is present in (b) obtained at $\mu = 0.25$ and $L = 16$, extrapolating the phase diagram using different system sizes, shown in (d), reveals the survival of this phase at $L = \infty$.

Experimental measurement. We now address the signatures of the zero modes from the experimental point of view. In a tunneling experiment with a local probe [87–91], the conductance at zero bias $G(\omega = 0, n)$ depends on the probability of extracting (injecting) an electron in site n at energy ω as $dI/dV(n, \omega) \sim \sum_{\alpha} |\langle GS | c_n^{(\dagger)} | \Psi_{\alpha} \rangle|^2 \delta(\omega - E_{\alpha} + E_{GS})$, where $|GS\rangle$ is the ground state and $H|\Psi_{\alpha}\rangle = E_{\alpha}|\Psi_{\alpha}\rangle$ are the many-body excited states of the system. In the presence of topological degeneracy, the ground state presents zero mode excitations that distinguish different ground states. In that scenario, the zero bias conductance at site n can be written as $dI/dV(n, \omega = 0) \sim \Xi(n)$ where

$$\Xi(n) = \sum_{\alpha} |\langle \Psi_{\alpha} | c_n | GS \rangle|^2 + |\langle \Psi_{\alpha} | c_n^{\dagger} | GS \rangle|^2 \quad (13)$$

which directly images the probability of a local excitation between the ground state and its degenerate manifold. Here, α runs over the ground state manifold. In particular, $\Xi(n)$ allows one to directly observe the emergence of topological zero modes associated with the topological degeneracy of the ground state. With the previous quantity, the emergence of topological zero modes associated to the topological degeneracy of the non-Hermitian model can be directly imaged. We show in Fig. 5 the local correlator computed for the interacting non-Hermitian model for different system sizes. As the system becomes larger, an edge excitation emerges in the model, which in the thermodynamic limit leads to decoupled modes between the two edges; see also the SM [79]. The previous quantity has been directly imaged in the realization of the current model in the topological phase with $\delta = U = 0$ and $\eta \neq 0$ [87], and minimal a chain with $\Delta \neq 0$ [91].

Conclusion. To summarize, we have presented a family of non-Hermitian interacting models featuring different classes of topological degeneracies. While non-interacting non-Hermitian models can be studied with conventional methodologies, the inclusion of many-body interactions renders exploring non-Hermitian systems greatly challenging. Our manuscript establishes a family of solvable interacting non-Hermitian models, providing ideal systems for benchmarking methodologies to treat interacting non-Hermitian models. Besides showing the emergence of different topological phases in the solvable limit, we provided the many-body operators accounting for the topological degeneracy of the model. We showed how non-Hermiticity modifies topological many-body models, substantially impacting the topological phases of Hermitian systems. We benchmarked our analytical construction with exact numerical calculations of the full many-body system, demonstrating that even for finite systems, the emergence of topological modes and topological degeneracies can be observed. Our results establish a versatile family of models featuring interacting

topology, providing a starting point for higher dimensional solvable interacting models.

Acknowledgement. S.S. thanks Vittorio Paeno and Abolhassan Vaezi for helpful discussions. J.L.L. acknowledges the computational resources provided by the Aalto Science-IT project, and the financial support from the Academy of Finland Projects No. 331342 and No. 336243 and the Jane and Aatos Erkko Foundation.

Appendix A: Mapping the non-Hermitian interacting Kitaev chain into a noninteracting Hamiltonian

Following Refs. [15, 16], we now present the generalization of mapping our non-Hermitian interacting model into a non-interacting Hamiltonian when $t = \Delta$ and $\mu = 0$.

In the first step, we represent the fermion operators in terms of the spin operators, described by Pauli matrices, using the Jordan-Wigner transformation [14, 17, 18, 86, 92–94] given by $c_i = K_i \sigma_i^-$, $c_i^\dagger = \sigma_i^+ K_i^+$, and $2n_i - 1 = \sigma_i^z$ with $\sigma^\pm = \sigma^x \pm i\sigma^y$ and $K_i = \prod_{j < i} (-\sigma_j^z)$. As a result, the spin representation of the Hamiltonian in Eq. (1) casts

$$\mathcal{H} = \sum_j \left[-t_j \sigma_j^x \sigma_{j+1}^x + \tilde{U}_j \sigma_j^z \sigma_{j+1}^z \right], \quad (\text{S1})$$

where $\tilde{U}_j = U_j - i\delta_j$. As the XY spin model is exactly solvable [95], one can transform the above XZ spin model, which may not be exactly solvable, in Eq. (S1) into an XY model. For this purpose, we perform a $\pi/2$ spin rotation on all spin operators around the x axis using $R = \exp[-i\pi \sum_j \sigma_j^x/2]$ [17]. The subsequent Hamiltonian yields

$$\mathcal{H} = \sum_j \left[-t_j \sigma_j^x \sigma_{j+1}^x + \tilde{U}_j \sigma_j^y \sigma_{j+1}^y \right]. \quad (\text{S2})$$

To diagonalize this spin Hamiltonian, we introduce a second Jordan-Wigner transformation [15, 16, 96, 97] given by

$$\sigma_i^x = (f_i^\dagger + f_i) \exp \left[i\pi \sum_{i < j} f_i^\dagger f_i \right], \quad (\text{S3})$$

$$\sigma_i^y = -i(f_i^\dagger - f_i) \exp \left[i\pi \sum_{i < j} f_i^\dagger f_i \right], \quad (\text{S4})$$

$$\sigma_i^z = 2f_i^\dagger f_i - 1. \quad (\text{S5})$$

Using the above relations, we rewrite the XY spin model as a fermionic quadratic model, which reads

$$\mathcal{H} = \sum_j -t_j \left[f_{j+1}^\dagger f_j + f_j^\dagger f_{j+1} + f_j^\dagger f_{j+1}^\dagger + f_{j+1} f_j \right]$$

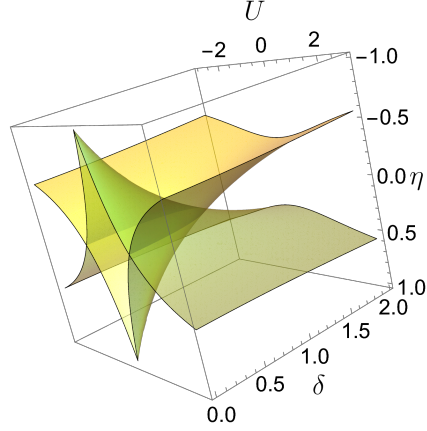


Figure S1. Phase boundaries of the effective Hamiltonian in Eq. (S12).

$$+ \sum_j \tilde{U}_j \left[f_{j+1}^\dagger f_j + f_j^\dagger f_{j+1} - f_j^\dagger f_{j+1}^\dagger - f_{j+1} f_j \right]. \quad (\text{S6})$$

As the bulk-boundary correspondence is not violated in our non-Hermitian system, searching for the presence of zero modes can be done in the momentum space (k) using the Fourier transformation $f_k = \sum_j f_j \exp[ika]$ with $a (= 1)$ be the lattice constant.

The quadratic Hamiltonian in the momentum space on a bipartite unit cell with sublattices (A, B) casts

$$\begin{aligned} \mathcal{H} = & \sum_k (-t + \tilde{U}) \left[z_k f_{kB}^\dagger f_{kA} + z_k^* f_{kA}^\dagger f_{kB} \right] \\ & - \sum_k (t + \tilde{U}) \left[w_k f_{-kA}^\dagger f_{kB}^\dagger + w_k^* f_{kB} f_{-kA} \right]. \end{aligned} \quad (\text{S7})$$

Here $\tilde{U} = U - i\delta$ and z_k and w_k read

$$z_k = (1 + \eta) + e^{-ika}(1 - \eta), \quad (\text{S8})$$

$$w_k = (1 + \eta) - e^{-ika}(1 - \eta). \quad (\text{S9})$$

The non-Hermitian Hamiltonian in Eq. (S7) can be written in a matrix form using the vector operator $\mathcal{C}_k^\dagger = (f_{kA}^\dagger, f_{kB}^\dagger, f_{-kA}, f_{-kB})$ as

$$\mathcal{H} = \frac{1}{2} \sum_k \mathcal{C}_k^\dagger \begin{pmatrix} 0 & a_1 z_k^* & 0 & a_2 w_k^* \\ a_1 z_k & 0 & -a_2 w_k & 0 \\ 0 & -a_2 w_k^* & 0 & -a_1 z_k^* \\ a_2 w_k & 0 & -a_1 z_k & 0 \end{pmatrix} \mathcal{C}_k, \quad (\text{S10})$$

where $a_1 = -t + \tilde{U}$ and $a_2 = -(t + \tilde{U})$. Expressing $\mathcal{H} = \frac{1}{2} \sum_k \Lambda_k \mathcal{C}_k^\dagger \mathcal{C}_k$, four eigenvalues Λ_k then read

$$\frac{\Lambda_k^2}{4} = \begin{cases} \tilde{U}^2(1 + \eta)^2 + t^2(1 - \eta)^2 - 2t\tilde{U}(1 - \eta^2) \cos(ka), \\ \tilde{U}^2(1 - \eta)^2 + t^2(1 + \eta)^2 - 2t\tilde{U}(1 - \eta^2) \cos(ka), \end{cases} \quad (\text{S11})$$

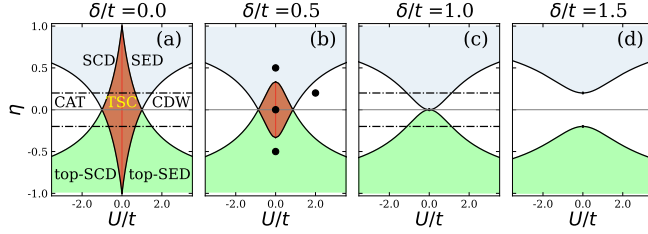


Figure S2. Phase diagrams of the non-Hermitian Hamiltonian in Eq. (S12) at $\mu = 0$ on the $(U/t - \eta)$ plane for $\delta/t = 0.0$ (a), 0.5 (b), 1.0 (c) and 1.5 (d). At $\delta = 0$, the phase diagram consists of seven phases, including the topological superconducting (TSC), (topological) superconducting dimer ((top-)SCD), (topological) single-electron dimer ((top-)SED), charge density wave (CDW), and Schrödinger cat (CAT) phases. Dashed dotted lines in (a) and (c) are at $\eta = \pm 0.2$. The circle points in (b) are located at $(U/t, \eta) \in \{(0, 0), (0, -0.5), (0, 0.5), (2.0, 0.2)\}$.

where $\tilde{U}^2 = U^2 - \delta^2 - 2i\delta U$. The gap closure in Λ_k occurs when we impose $\text{Re}[\Lambda_k] = 0$ resulting in

$$\frac{U}{t} = \sqrt{\frac{\delta^2}{t^2} - \frac{(1 \pm \eta)^2}{(1 \mp \eta)^2}}, \quad (\text{S12})$$

which is obtained at $k = \pm\pi/2$. We emphasize that due to the charge conjugation symmetry enforcing $\text{Re}[\Lambda_k] = 0$ ensures $\text{Im}[\Lambda_k] = 0$.

While Eq. (S12) determines phase boundaries, we note that characterizing the properties of each phase cannot be addressed from the spectra of the Hamiltonian in Eq. (S10). This is because the topological character of various phases may not be preserved after performing nonlocal (Wigner) transformations [15, 84]. Nevertheless, as non-Hermiticity does not violate the bulk-boundary correspondence, we can deduce some pieces of information regarding zero modes from effective noninteracting Hamiltonians.

For this purpose, we start with presenting the phase boundaries in Eq. (S12) as a function of (η, U, δ) in Fig. S1. The two-dimensional intersection of this phase boundaries at $\delta = 0.0$ (a), 0.5 (b), 1.0 (c), and 1.5 (d) is shown in Fig. S2. The Hermitian phase diagram in Fig. S2(a) comprises seven phases including the topological superconducting (TSC), (topological) superconducting dimer ((top-)SCD), (topological) single-electron dimer ((top-)SED), charge density wave (CDW), and Schrödinger cat (CAT) phases [15]. The CAT phase is a superposition of two superconducting states [15, 17].

To explore the zero modes in the phase diagram, we now look at the spectra of the system with an open boundary condition at $\mu = 0$. We first consider the Hermitian limit with $\delta = 0.0$ and at $\eta \pm 0.2$ along the cuts shown by dashed-dotted lines in Fig. S2. The associated spectra for $\eta = -0.2(0.2)$ are shown in Fig. S3. Comparing two pairs of smallest absolute values of eigenvalues in (a, b), shown in red and blue, we realize that

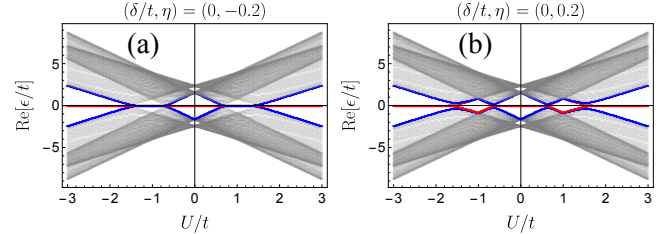


Figure S3. Spectra of the Hermitian Hamiltonian as a function of U/t at $\mu = \delta = 0$ and $\eta = -0.2$ (a) and 0.2 (b). Two pairs of the smallest absolute values of eigenvalues are shown in red and blue.

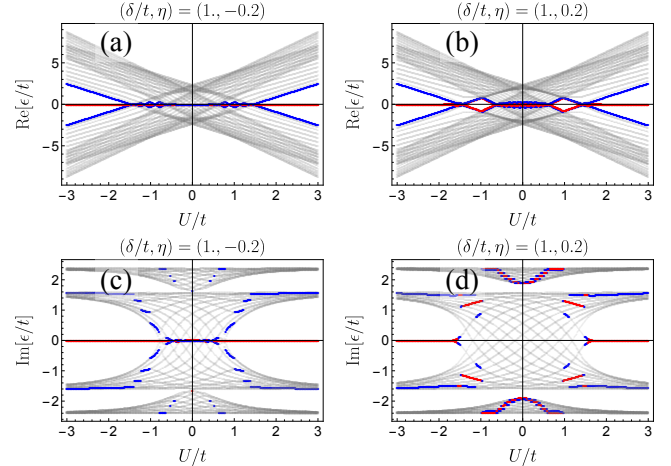


Figure S4. Real(a,b) and imaginary (c,d) parts of the spectra as a function of U/t at $\mu = 0$, $\delta = 1.0$ and $\eta = -0.2$ (a,c) and 0.2 (b,d). Two pairs of the smallest absolute values of eigenvalues are shown in red and blue.

the CDW, CAT, and TSC phases are twofold degenerate. The spectra also exhibit fourfold degeneracies in top-SCD and top-SED; see panel (a). However, these fourfold degeneracies are lifted for $\eta > 0$ in the SCD and SED phases; see panel (b).

Further looking at Fig. S2 reveals that the boundaries of the TSC phase shrink toward diminishing this phase as δ increases. Reducing the regions with the TSC phase results in lifting the separation between pairs of phases, namely (top-SCD, top-SED), (SCD, SED), and (CAT, CDW). As the order of degeneracies in both components of these pairs are identical, we still detect fourfold, twofold, and no degeneracies, respectively, in the green, white, and blue regions in all panels of Fig. S2. This can be seen in the spectra of the system at $\delta = 1.0$ along cuts at $\eta = \pm 0.2$ in Fig. S4. Note that the real and imaginary parts of eigenvalues are zero at degenerate points due to the particle-hole symmetry in the system.

Aside from $2n$ -fold degeneracies with $n \in \{0, 1, 2\}$, each non-Hermitian phase in Fig. S2 exhibits a particular non-Hermitian gap in their spectrum. We demonstrate this point by plotting the complex spectra of systems belonging to the brown, blue, lime, and white regions,

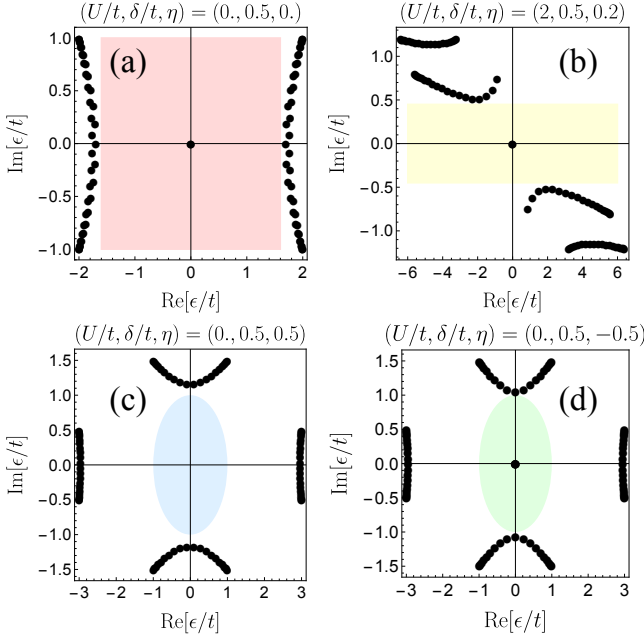


Figure S5. Spectra at $\mu = 0$, $\delta = 0.5$ and $(U/t, \eta) = (0, 0)$ (a), $(2, 0.2)$ (b), $(0, -0.5)$ (c), and $(0, 0.5)$ (d). The real (imaginary) line gaps are shown in red (yellow). The point gap is shown by a circle with a unit radius.

shown by circle points in Fig. S2(b). In the TSC phases, the spectrum displays a real line gap shown by a red rectangle in Fig. S5 (a). The spectra exhibit the imaginary line gap within the CDW and CAT phases as exemplified in Fig S5(b). The gap becomes the point gap both in phases with fourfold or no degeneracies, e.g., in the top-SED shown in Fig S5(c) and in the SED phase presented in Fig. S5(d).

Appendix B: Topological modes in the thermodynamic limit

In the previous sections, we have focused on relatively small-length systems that can be solved with exact diagonalization. In this section, we show that the edge modes associated with topological degeneracies evolve into fully decoupled modes in the thermodynamic limit. In order to surpass the length limitations of exact diagonalization, in this section, we solve the interacting quantum many-body model using a non-Hermitian tensor network formalism [98–100], targeting the ground state and lowest excited states [61, 67]. We show in Fig. S6 the spatially resolved correlator computed with the non-Hermitian tensor network formalism. It is observed that as the system becomes larger, the local edge modes become more decoupled (Fig. S6(a)), giving rise to fully decoupled modes for large systems; see panels (b) and (c) in Fig. S6.

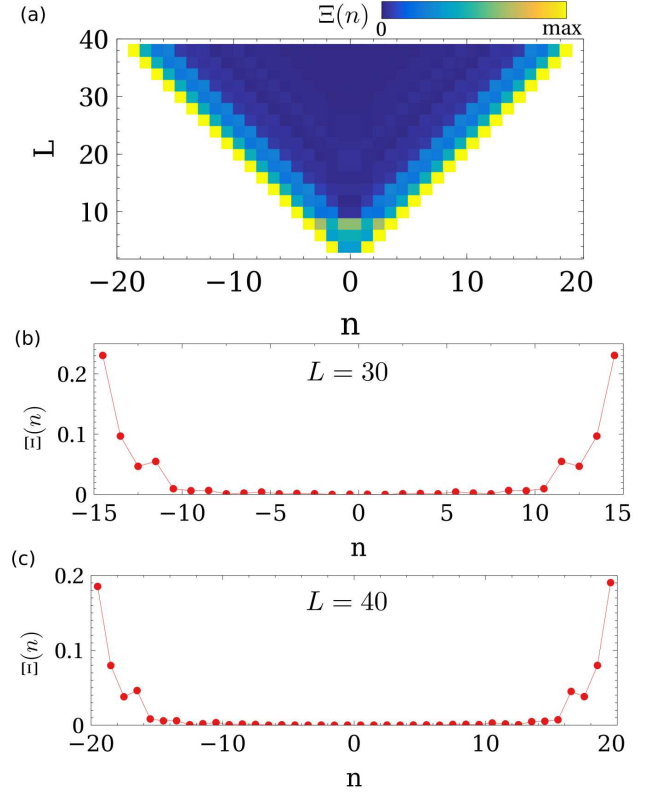


Figure S6. Spatially resolved local correlators, showing the emergence of edge modes. Panel (a) shows the scaling with the length of the system, highlighting the emergence of decoupled modes for large lengths. Panels (b,c) show the spatially resolved correlators for two specific lengths, showing the localization of the excitations on the edges. We set $U = 0.5t$, $\Delta = t$, $\mu = 0.25t$, $\delta = 0.5t$ and $\eta = 0$.

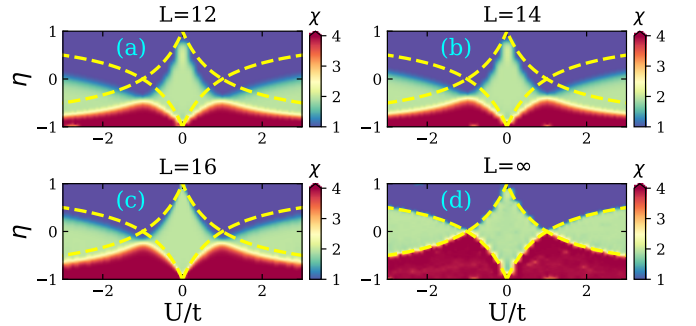


Figure S7. Degeneracy of the non-Hermitian model for different system sizes, $L = 12$ (a), $L = 14$ (b) and $L = 16$ (c), and extrapolation in the thermodynamic limit (d). It is observed that while for finite systems, finite size effects affect the inferred boundaries between different phases, the extrapolation scheme allows to the recovery of the correct phase diagram. The yellow dashed lines display the exact phase boundaries. We took $\Delta = t$, $\delta = \mu = 0$, and $\lambda = 0.01t$.

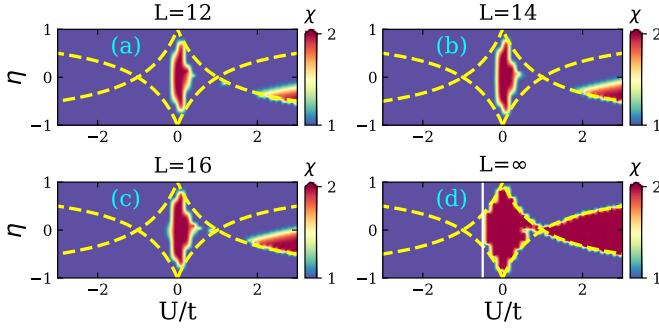


Figure S8. Degeneracy of the non-Hermitian model for different system sizes, $L = 12$ (a), $L = 14$ (b) and $L = 16$ (c), and extrapolation in the thermodynamic limit (d) with $\Delta = t$, $\delta = 0$, $\mu = 0.25t$, and $\lambda = 0.01t$. The vertical white line in (d) is at $U = -0.5t$.

Appendix C: Finite size effects and extrapolation to the thermodynamic limit

In the main text, we have focused on studying the case of finite systems numerically. Due to finite size effects, the degeneracy of the ground state is lifted due to the coupling of the topological excitations. In order to extract the topological degeneracy in the thermodynamic limit, a finite size scaling of the energy splittings can be performed. In this section, we show that with a size scaling, we can recover the exact analytic results in the interacting limit from exact numerical calculations in finite systems. The finite size scaling relies on taking a scaling for the excited state energies as $\epsilon_\alpha(L) = a_\alpha + b_\alpha/L$, so that in the thermodynamic limit $\epsilon_\alpha(L = \infty) = a_\alpha$. The excited state energies are taken as $\epsilon_\alpha = |E_\alpha - E_0|$, where E_α is the complex eigenenergy of the many-body Hamiltonian and E_0 the ground state energy. By computing the energies for a set of finite-size systems, the coefficients a, b can be extracted, and the energies in the thermodynamic limit are obtained. With the extracted

energy differences, the degeneracy of the ground state can be computed as $\chi = \sum_\alpha e^{-\lambda\epsilon_\alpha}$ with λ being the energy smearing.

We present in Fig. S7 how this methodology allows obtaining the degeneracies in the thermodynamic limit. It is observed that for finite-size systems, the phase boundaries are substantially shifted and are size dependent; see panels (a), (b), and (c) in Fig. S7. Using the extrapolation scheme noted above, the correct phase boundaries known from the analytic solution are recovered, as shown in Fig. S7(d).

We further perform a similar extrapolation scheme to the Hermitian phase diagram at $\mu = 0.25t$. Here we employ the exact diagonalization methods in Fig. S8 and the tensor-network formalism in Fig. S9. As it is evident, increasing the length of the chain in panels (a)-(c) results in improving the boundaries of twofold degenerate topological phases. In the thermodynamic limit, the extrapolated phase diagrams, presented in Fig. S8(d) and

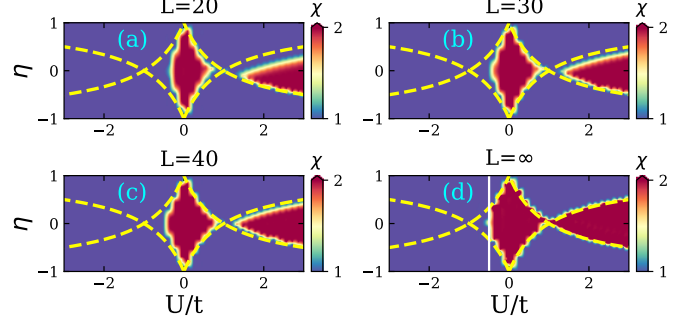


Figure S9. Degeneracy of the non-Hermitian model obtained from the DMRG calculations for different system sizes, $L = 20$ (a), $L = 30$ (b) and $L = 40$ (c), and extrapolation in the thermodynamic limit (d) with $\Delta = t$, $\delta = 0$, $\mu = 0.25t$ and $\lambda = 0.01t$. The vertical white line in (d) is at $U = -0.5t$.

Fig. S9(d), recover the exact phase boundaries at $\mu = 0$ and $U \geq -0.5t$. We note that the phase boundary at $\eta = 0$ is located at $U = -0.5t$ (vertical white line), in agreement with the previous Hermitian calculations [86].

-
- [1] Tohru Koma and Hal Tasaki, “Symmetry breaking and finite-size effects in quantum many-body systems,” *Journal of Statistical Physics* **76**, 745–803 (1994).
- [2] Spartak T. Belyaev, “Many-body physics and spontaneous symmetry breaking,” *International Journal of Modern Physics B* **20**, 2579–2590 (2006), <https://doi.org/10.1142/S0217979206035059>.
- [3] Tomas Brauner, “Spontaneous symmetry breaking and nambu–goldstone bosons in quantum many-body systems,” *Symmetry* **2**, 609–657 (2010).
- [4] Guo-Hui Dong, Yi-Nan Fang, and Chang-Pu Sun, “Quantifying spontaneously symmetry breaking of quantum many-body systems*,” *Communications in Theoretical Physics* **68**, 405 (2017).
- [5] Lea F. Santos, Marco Távora, and Francisco Pérez-Bernal, “Excited-state quantum phase transitions in many-body systems with infinite-range interaction: Localization, dynamics, and bifurcation,” *Phys. Rev. A* **94**, 012113 (2016).
- [6] Markus Heyl, “Dynamical quantum phase transitions: a review,” *Reports on Progress in Physics* **81**, 054001 (2018).
- [7] Angelo Carollo, Davide Valenti, and Bernardo Spagnolo, “Geometry of quantum phase transitions,” *Physics Reports* **838**, 1–72 (2020).
- [8] T. Serwatka, R. G. Melko, A. Burkov, and P.-N. Roy, “Quantum phase transition in the one-dimensional water chain,” *Phys. Rev. Lett.* **130**, 026201 (2023).
- [9] Guo-Qing Zhang, Dan-Wei Zhang, Zhi Li, Z. D. Wang, and Shi-Liang Zhu, “Statistically related many-

- body localization in the one-dimensional anyon hubbard model,” *Physical Review B* **102** (2020), 10.1103/physrevb.102.054204.
- [10] M. Hashisaka, T. Jonckheere, T. Akiho, S. Sasaki, J. Rech, T. Martin, and K. Muraki, “Andreev reflection of fractional quantum hall quasiparticles,” *Nature Communications* **12** (2021), 10.1038/s41467-021-23160-6.
- [11] Vilja Kaskela and J. L. Lado, “Dynamical topological excitations in parafermion chains,” *Phys. Rev. Res.* **3**, 013095 (2021).
- [12] Jurriaan Wouters, Fabian Hassler, Hosho Katsura, and Dirk Schuricht, “Phase diagram of an extended parafermion chain,” *SciPost Phys. Core* **5**, 008 (2022).
- [13] Suhas Gangadharaiah, Bernd Braunecker, Pascal Simon, and Daniel Loss, “Majorana edge states in interacting one-dimensional systems,” *Phys. Rev. Lett.* **107**, 036801 (2011).
- [14] Hosho Katsura, Dirk Schuricht, and Masahiro Takahashi, “Exact ground states and topological order in interacting kitaev/majorana chains,” *Phys. Rev. B* **92**, 115137 (2015).
- [15] Motohiko Ezawa, “Exact solutions and topological phase diagram in interacting dimerized Kitaev topological superconductors,” *Physical Review B* **96**, 1–5 (2017), arXiv:1707.03983.
- [16] Yucheng Wang, Jian Jian Miao, Hui Ke Jin, and Shu Chen, “Characterization of topological phases of dimerized Kitaev chain via edge correlation functions,” *Physical Review B* **96** (2017), 10.1103/PhysRevB.96.205428, arXiv:1708.03891.
- [17] Jian-Jian Miao, Hui-Ke Jin, Fu-Chun Zhang, and Yi Zhou, “Exact solution for the interacting kitaev chain at the symmetric point,” *Phys. Rev. Lett.* **118**, 267701 (2017).
- [18] A. A. Zvyagin, “Charging of majorana edge modes caused by interaction: Exact results,” *Phys. Rev. B* **105**, 115406 (2022).
- [19] HQ Lin, “Exact diagonalization of quantum-spin models,” *Physical Review B* **42**, 6561 (1990).
- [20] Guifré Vidal, “Efficient simulation of one-dimensional quantum many-body systems,” *Phys. Rev. Lett.* **93**, 040502 (2004).
- [21] U. Schollwöck, “The density-matrix renormalization group,” *Rev. Mod. Phys.* **77**, 259–315 (2005).
- [22] G. Kotliar, S. Y. Savrasov, K. Haule, V. S. Oudovenko, O. Parcollet, and C. A. Marianetti, “Electronic structure calculations with dynamical mean-field theory,” *Rev. Mod. Phys.* **78**, 865–951 (2006).
- [23] E. M. Stoudenmire, Jason Alicea, Oleg A. Starykh, and Matthew P.A. Fisher, “Interaction effects in topological superconducting wires supporting majorana fermions,” *Phys. Rev. B* **84**, 014503 (2011).
- [24] Pietro Silvi, Ferdinand Tschirsich, Matthias Gerster, Johannes Jünemann, Daniel Jaschke, Matteo Rizzi, and Simone Montangero, “The tensor networks anthology: Simulation techniques for many-body quantum lattice systems,” *SciPost Physics Lecture Notes* , 008 (2019).
- [25] Riku Tuovinen, “Electron correlation effects in superconducting nanowires in and out of equilibrium,” *New Journal of Physics* **23** (2021), 10.1088/1367-2630/ac1898, arXiv:2105.06193.
- [26] Kenta Esaki, Masatoshi Sato, Kazuki Hasebe, and Mahito Kohmoto, “Edge states and topological phases in non-hermitian systems,” *Phys. Rev. B* **84**, 205128 (2011).
- [27] Simon Malzard, Charles Poli, and Henning Schomerus, “Topologically protected defect states in open photonic systems with non-hermitian charge-conjugation and parity-time symmetry,” *Phys. Rev. Lett.* **115**, 200402 (2015).
- [28] Zongping Gong, Yuto Ashida, Kohei Kawabata, Kazuaki Takasan, Sho Higashikawa, and Masahito Ueda, “Topological phases of non-hermitian systems,” *Phys. Rev. X* **8**, 031079 (2018).
- [29] Shunyu Yao and Zhong Wang, “Edge states and topological invariants of non-hermitian systems,” *Phys. Rev. Lett.* **121**, 086803 (2018).
- [30] Huitao Shen, Bo Zhen, and Liang Fu, “Topological band theory for non-hermitian hamiltonians,” *Phys. Rev. Lett.* **120**, 146402 (2018).
- [31] Kohei Kawabata, Ken Shiozaki, Masahito Ueda, and Masatoshi Sato, “Symmetry and topology in non-hermitian physics,” *Phys. Rev. X* **9**, 041015 (2019).
- [32] Kazuki Yokomizo and Shuichi Murakami, “Non-bloch band theory of non-hermitian systems,” *Phys. Rev. Lett.* **123**, 066404 (2019).
- [33] Hengyun Zhou and Jong Yeon Lee, “Periodic table for topological bands with non-hermitian symmetries,” *Phys. Rev. B* **99**, 235112 (2019).
- [34] Dan S. Borgnia, Alex Jura Kruchkov, and Robert-Jan Slager, “Non-hermitian boundary modes and topology,” *Phys. Rev. Lett.* **124**, 056802 (2020).
- [35] Yuto Ashida, Zongping Gong, and Masahito Ueda, “Non-hermitian physics,” *Advances in Physics* **69**, 249–435 (2020).
- [36] Sharareh Sayyad, Julia D. Hannukainen, and Adolfo G. Grushin, “Non-hermitian chiral anomalies,” *Phys. Rev. Res.* **4**, L042004 (2022).
- [37] Nobuyuki Okuma and Masatoshi Sato, “Non-hermitian topological phenomena: A review,” *Annual Review of Condensed Matter Physics* **14**, null (2023), <https://doi.org/10.1146/annurev-conmatphys-040521-033133>.
- [38] Tomaz Prosen, “Third quantization: a general method to solve master equations for quadratic open fermi systems,” *New Journal of Physics* **10**, 043026 (2008).
- [39] Simon Lieu, Max McGinley, and Nigel R. Cooper, “Tenfold way for quadratic lindbladians,” *Phys. Rev. Lett.* **124**, 040401 (2020).
- [40] Sharareh Sayyad, Jinlong Yu, Adolfo G. Grushin, and Lukas M. Sieberer, “Entanglement spectrum crossings reveal non-hermitian dynamical topology,” *Phys. Rev. Res.* **3**, 033022 (2021).
- [41] Jan Perina Jr, Adam Miranowicz, Grzegorz Chimczak, and Anna Kowalewska-Kudłaszyk, “Quantum liouvillian exceptional and diabolical points for bosonic fields with quadratic hamiltonians: The heisenberg-langevin equation approach,” *Quantum* **6**, 883 (2022).
- [42] Fan Yang, Qing-Dong Jiang, and Emil J. Bergholtz, “Liouvillian skin effect in an exactly solvable model,” *Phys. Rev. Res.* **4**, 023160 (2022).
- [43] Spenser Talkington and Martin Claassen, “Dissipation-induced flat bands,” *Phys. Rev. B* **106**, L161109 (2022).
- [44] Elias Starchl and Lukas M. Sieberer, “Relaxation to a parity-time symmetric generalized gibbs ensemble after a quantum quench in a driven-dissipative kitaev chain,” *Phys. Rev. Lett.* **129**, 220602 (2022).

- [45] Clemens Gneiting, Akshay Koottandavida, A. V. Rozhkov, and Franco Nori, “Unraveling the topology of dissipative quantum systems,” *Phys. Rev. Res.* **4**, 023036 (2022).
- [46] Weijian Chen, Maryam Abbasi, Yogesh N. Joglekar, and Kater W. Murch, “Quantum jumps in the non-hermitian dynamics of a superconducting qubit,” *Phys. Rev. Lett.* **127**, 140504 (2021).
- [47] Maryam Abbasi, Weijian Chen, Mahdi Naghiloo, Yogesh N. Joglekar, and Kater W. Murch, “Topological quantum state control through exceptional-point proximity,” *Phys. Rev. Lett.* **128**, 160401 (2022).
- [48] Weijian Chen, Maryam Abbasi, Byung Ha, Serra Erdamar, Yogesh N. Joglekar, and Kater W. Murch, “Decoherence-induced exceptional points in a dissipative superconducting qubit,” *Phys. Rev. Lett.* **128**, 110402 (2022).
- [49] Daniel Leykam, Konstantin Y. Bliokh, Chunli Huang, Y. D. Chong, and Franco Nori, “Edge modes, degeneracies, and topological numbers in non-hermitian systems,” *Phys. Rev. Lett.* **118**, 040401 (2017).
- [50] Emil J. Bergholtz, Jan Carl Budich, and Flore K. Kunst, “Exceptional topology of non-hermitian systems,” *Rev. Mod. Phys.* **93**, 015005 (2021).
- [51] Sharareh Sayyad and Flore K. Kunst, “Realizing exceptional points of any order in the presence of symmetry,” *Phys. Rev. Research* **4**, 023130 (2022).
- [52] Sharareh Sayyad, Marcus Stalhammar, Lukas Rodland, and Flore K Kunst, “Symmetry-protected exceptional and nodal points in non-hermitian systems,” arXiv:2204.13945 (2022).
- [53] Sharareh Sayyad, “Protection of all nondefective twofold degeneracies by antiunitary symmetries in non-hermitian systems,” *Physical Review Research* **4**, 043213 (2022).
- [54] Fei Song, Shunyu Yao, and Zhong Wang, “Non-hermitian skin effect and chiral damping in open quantum systems,” *Phys. Rev. Lett.* **123**, 170401 (2019).
- [55] Xiujuan Zhang, Tian Zhang, Ming-Hui Lu, and Yan-Feng Chen, “A review on non-hermitian skin effect,” *Advances in Physics: X* **7**, 2109431 (2022), <https://doi.org/10.1080/23746149.2022.2109431>.
- [56] Roland W Freund, “Quasi-kernel polynomials and their use in non-hermitian matrix iterations,” *Journal of Computational and Applied Mathematics* **43**, 135–158 (1992).
- [57] Roland W Freund, Martin H Gutknecht, and Noël M Nachtigal, “An implementation of the look-ahead lanczos algorithm for non-hermitian matrices,” *SIAM journal on scientific computing* **14**, 137–158 (1993).
- [58] Zhen Guo, Zheng-Tao Xu, Meng Li, Li You, and Shuo Yang, “Variational matrix product state approach for non-hermitian system based on a companion hermitian hamiltonian,” arXiv:2210.14858 (2022), arXiv:2210.14858.
- [59] Russell Carden, *Ritz values and Arnoldi convergence for non-Hermitian matrices* (Rice University, 2011).
- [60] Jianhua Zhang and Hua Dai, “Global gpbicg method for complex non-hermitian linear systems with multiple right-hand sides,” *Computational and Applied Mathematics* **35**, 171–185 (2016).
- [61] Guangze Chen, Fei Song, and Jose L. Lado, “Topological spin excitations in non-Hermitian spin chains with a generalized kernel polynomial algorithm,” *arXiv* (2022), 10.48550/arXiv.2208.06425, arXiv:2208.06425.
- [62] Takahiro Fukui and Norio Kawakami, “Breakdown of the Mott insulator: Exact solution of an asymmetric Hubbard model,” *Physical Review B - Condensed Matter and Materials Physics* **58**, 16051–16056 (1998), arXiv:9806023 [cond-mat].
- [63] Berislav Buća, Cameron Booker, Marko Medenjak, and Dieter Jaksch, “Bethe ansatz approach for dissipation: exact solutions of quantum many-body dynamics under loss,” *New Journal of Physics* **22**, 123040 (2020).
- [64] X. Z. Zhang and Z. Song, “ η -pairing ground states in the non-hermitian hubbard model,” *Phys. Rev. B* **103**, 235153 (2021).
- [65] Masaya Nakagawa, Norio Kawakami, and Masahito Ueda, “Exact liouvillian spectrum of a one-dimensional dissipative hubbard model,” *Phys. Rev. Lett.* **126**, 110404 (2021).
- [66] Hironobu Yoshida and Hoshio Katsura, “Exact analysis of the Liouvillian gap and dynamics in the dissipative $SU(N)$ Fermi-Hubbard model,” , 1–7 (2022), arXiv:2209.03743.
- [67] Timo Hyart and J. L. Lado, “Non-hermitian many-body topological excitations in interacting quantum dots,” *Phys. Rev. Res.* **4**, L012006 (2022).
- [68] Kazuki Yamamoto, Masaya Nakagawa, Masaki Tezuka, Masahito Ueda, and Norio Kawakami, “Universal properties of dissipative tomonaga-luttinger liquids: Case study of a non-hermitian xxz spin chain,” *Phys. Rev. B* **105**, 205125 (2022).
- [69] Ya-Nan Wang, Wen-Long You, and Gaoyong Sun, “Quantum criticality in interacting bosonic kitaev-hubbard models,” *Phys. Rev. A* **106**, 053315 (2022).
- [70] Maciej Lewenstein, Anna Sanpera, Veronica Ahufinger, Bogdan Damski, Aditi Sen(De), and Ujjwal Sen, “Ultracold atomic gases in optical lattices: mimicking condensed matter physics and beyond,” *Advances in Physics* **56**, 243–379 (2007), <https://doi.org/10.1080/00018730701223200>.
- [71] Qi Zhang, Minhan Lou, Xinwei Li, John L. Reno, Wei Pan, John D. Watson, Michael J. Manfra, and Junichiro Kono, “Collective non-perturbative coupling of 2D electrons with high-quality-factor terahertz cavity photons,” *Nature Physics* **12**, 1005–1011 (2016), arXiv:1604.08297 [cond-mat.quant-gas].
- [72] Christian Gross and Immanuel Bloch, “Quantum simulations with ultracold atoms in optical lattices,” *Science* **357**, 995–1001 (2017), <https://www.science.org/doi/pdf/10.1126/science.aa13837>.
- [73] Lorenzo Rosso, Leonardo Mazza, and Alberto Biella, “Eightfold way to dark states in $SU(3)$ cold gases with two-body losses,” *Physical Review A* **105**, 1–6 (2022).
- [74] Diego Rainis and Daniel Loss, “Majorana qubit decoherence by quasiparticle poisoning,” *Phys. Rev. B* **85**, 174533 (2012).
- [75] Simon Lieu, “Non-hermitian majorana modes protect degenerate steady states,” *Phys. Rev. B* **100**, 085110 (2019).
- [76] Tetsuro Sakaguchi, Hiroto Nishijima, and Yositake Takane, “Bulk-boundary correspondence and boundary zero modes in a non-hermitian kitaev chain model,” *Journal of the Physical Society of Japan* **91**, 124711 (2022), <https://doi.org/10.7566/JPSJ.91.124711>.
- [77] Fabian Hassler and Dirk Schuricht, “Strongly interacting majorana modes in an array of josephson junctions,”

- New Journal of Physics* **14**, 125018 (2012).
- [78] Yogesh N. Joglekar and Andrew K. Harter, “Passive parity-time-symmetry-breaking transitions without exceptional points in dissipative photonic systems,” *Photon. Res.* **6**, A51–A57 (2018).
- [79] The Supplemental Material includes details on mapping the non-Hermitian interacting Kitaev chain into a non-interacting Hamiltonian and discussions on the thermodynamic limits of topological modes and topological boundaries.
- [80] A Yu Kitaev, “Unpaired majorana fermions in quantum wires,” *Physics-Uspekhi* **44**, 131–136 (2001).
- [81] G. Goldstein and C. Chamon, “Exact zero modes in closed systems of interacting fermions,” *Physical Review B - Condensed Matter and Materials Physics* **86**, 1–5 (2012), arXiv:1108.1734.
- [82] Guang Yang and D. E. Feldman, “Exact zero modes and decoherence in systems of interacting Majorana fermions,” *Physical Review B - Condensed Matter and Materials Physics* **89**, 1–12 (2014), arXiv:1311.7604.
- [83] G. Kells, “Multiparticle content of Majorana zero modes in the interacting p -wave wire,” *Physical Review B - Condensed Matter and Materials Physics* **92**, 1–15 (2015), arXiv:1507.06539.
- [84] Max McGinley, Johannes Knolle, and Andreas Nunnenkamp, “Robustness of Majorana edge modes and topological order: Exact results for the symmetric interacting Kitaev chain with disorder,” *Physical Review B* **96**, 1–5 (2017), arXiv:1706.10249.
- [85] Paul Fendley, “Parafermionic edge zero modes in Zn-invariant spin chains,” *Journal of Statistical Mechanics: Theory and Experiment* **2012** (2012), 10.1088/1742-5468/2012/11/P11020, arXiv:1209.0472.
- [86] Iman Mahyaeh and Eddy Ardonne, “Study of the phase diagram of the Kitaev-Hubbard chain,” *Physical Review B* **101**, 85125 (2020).
- [87] Robert Drost, Teemu Ojanen, Ari Harju, and Peter Liljeroth, “Topological states in engineered atomic lattices,” *Nature Physics* **13**, 668–671 (2017).
- [88] S. N. Kempkes, M. R. Slot, J. J. van den Broeke, P. Capiod, W. A. Benalcazar, D. Vanmaekelbergh, D. Bercioux, I. Swart, and C. Morais Smith, “Robust zero-energy modes in an electronic higher-order topological insulator,” *Nature Materials* **18**, 1292–1297 (2019).
- [89] S. N. Kempkes, M. R. Slot, S. E. Freeney, S. J. M. Zevenhuizen, D. Vanmaekelbergh, I. Swart, and C. Morais Smith, “Design and characterization of electrons in a fractal geometry,” *Nature Physics* **15**, 127–131 (2018).
- [90] Md Nurul Huda, Shawlienu Kezilebieke, Teemu Ojanen, Robert Drost, and Peter Liljeroth, “Tunable topological domain wall states in engineered atomic chains,” *npj Quantum Materials* **5** (2020), 10.1038/s41535-020-0219-3.
- [91] Tom Dvir, Guanzhong Wang, Nick van Loo, Chun-Xiao Liu, Grzegorz P. Mazur, Alberto Bordin, Sebastiaan L. D. ten Haaf, Ji-Yin Wang, David van Driel, Francesco Zatelli, Xiang Li, Filip K. Malinowski, Sasa Gazibegovic, Ghada Badawy, Erik P. A. M. Bakkers, Michael Wimmer, and Leo P. Kouwenhoven, “Realization of a minimal kитаev chain in coupled quantum dots,” *Nature* **614**, 445–450 (2023).
- [92] Eran Sela, Alexander Altland, and Achim Rosch, “Majorana fermions in strongly interacting helical liquids,” *Phys. Rev. B* **84**, 085114 (2011).
- [93] Yu-Guo Liu, Lu Xu, and Zhi Li, “Quantum phase transition in a non-hermitian XY spin chain with global complex transverse field,” *Journal of Physics: Condensed Matter* **33**, 295401 (2021).
- [94] Shihao Bi, Yan He, and Peng Li, “Ring-frustrated non-hermitian XY model,” *Physics Letters A* **395**, 127208 (2021).
- [95] T. D. Schultz, D. C. Mattis, and E. H. Lieb, “Two-dimensional ising model as a soluble problem of many fermions,” *Rev. Mod. Phys.* **36**, 856–871 (1964).
- [96] Lin-Jie Ding and Yuan Zhong, “Gruneisen ratio quest for self-duality of quantum criticality in a spin-1/2 XY chain with dzyaloshinskii-moriya interaction,” *Communications in Theoretical Physics* **73**, 095701 (2021).
- [97] Kazuhiro Wada, Takanori Sugimoto, and Takami Tohyama, “Coexistence of strong and weak Majorana zero modes in an anisotropic XY spin chain with second-neighbor interactions,” *Physical Review B* **104**, 1–12 (2021), arXiv:2103.12281.
- [98] DMRGPy Library <https://github.com/joselado/dmrgpy>.
- [99] ITensor Library <http://itensor.org>.
- [100] Matthew Fishman, Steven R. White, and E. Miles Stoudenmire, “The ITensor Software Library for Tensor Network Calculations,” *SciPost Phys. Codebases* , 4 (2022).